Geosci. Model Dev. Discuss., 7, 2249–2291, 2014
www.geosci-model-dev-discuss.net/7/2249/2014/
doi:10.5194/gmdd-7-2249-2014

Geoscientific Model Development Discussions
Open Access

Improving subtropical boundary layer cloudiness in the 2011 NCEP GFS

J. K. Fletcher[1], C. S. Bretherton[2], H. Xiao[3], R. Sun[4], and J. Han[5]

[1]Monash University, Clayton, Victoria, Australia
[2]University of Washington, Seattle, Washington, USA
[3]Pacific Northwest National Laboratory, Richland, Washington, USA
[4]IMSG at NOAA/NWS/NCEP/EMC, Camp Springs, Maryland, USA
[5]SRG at NOAA/NWS/NCEP/EMC, Camp Springs, Maryland, USA

Received: 21 February 2014 – Accepted: 21 March 2014 – Published: 9 April 2014

Correspondence to: J. K. Fletcher (jennifer.fletcher@monash.edu)

Published by Copernicus Publications on behalf of the European Geosciences Union.

Abstract

The current operational version of National Centers for Environmental Prediction (NCEP) Global Forecasting System (GFS) shows significant low cloud bias. These biases also appear in the Coupled Forecast System (CFS), which is developed from the GFS. These low cloud biases degrade seasonal and longer climate forecasts, particularly of shortwave cloud radiative forcing, and affect predicted sea-surface temperature. Reducing this bias in the GFS will aid the development of future CFS versions and contributes to NCEP's goal of unified weather and climate modelling.

Changes are made to the shallow convection and planetary boundary layer parametrisations to make them more consistent with current knowledge of these processes and to reduce the low cloud bias. These changes are tested in a single-column version of GFS and in global simulations with GFS coupled to a dynamical ocean model. In the single column model, we focus on changing parameters that set the following: the strength of shallow cumulus lateral entrainment, the conversion of updraught liquid water to precipitation and grid-scale condensate, shallow cumulus cloud top, and the effect of shallow convection in stratocumulus environments. Results show that these changes improve the single-column simulations when compared to large eddy simulations, in particular through decreasing the precipitation efficiency of boundary layer clouds. These changes, combined with a few other model improvements, also reduce boundary layer cloud and albedo biases in global coupled simulations.

1 Introduction

The National Centers for Environmental Prediction (NCEP) Global Forecast System (GFS, http://www.emc.ncep.noaa.gov/GFS/doc.php) is an important model for operational weather forecasting. A frozen version of the GFS is coupled to the Modular Ocean Model v4 (http://www.gfdl.noaa.gov/mom-ocean-model) and called the Coupled Forecast System (CFS); this is used for seasonal to inter-decadal climate predictions

GMDD
7, 2249–2291, 2014

and reanalyses (Saha et al., 2006, 2010). An outstanding problem for both the GFS and CFS, described in more detail below, is the representation of boundary layer clouds. We focus on improving parametrisation of these clouds and their associated processes in the GFS, using insights gained from parametrisation development work in climate models and studies using large eddy simulation.

This research was conducted collaboratively by researchers at the University of Washington and NCEP, funded as part of a NOAA-funded Climate Process Team (CPT) on the Stratocumulus–Cumulus Transition. The purpose of the CPT was to improve the representation of subtropical boundary-layer cloud processes in the GFS and CFS, as well as in the Community Earth System Model (CESM, http://www.cesm.ucar.edu/), using the relative strengths and weaknesses of these two rather different modelling systems to help inform further parametrisation advances in both models. The CPT has also involved researchers from the Jet Propulsion Laboratory, University of California Los Angeles, the National Center for Atmospheric Research (NCAR), and Lawrence Livermore National Laboratories.

It is anticipated that Version 3 of the CFS will be developed from an upcoming operational version of the GFS, making current biases in the GFS relevant to forecasts of seasonal and longer timescales. Xiao et al. (2014) presented our CPT's comparisons of the simulated climate from multidecadal free-running simulations using an ocean-coupled version of the GFS operational in late 2011 with comparable simulations using Version 1 of the CESM (which uses the Community Atmosphere Model Version 5, or CAM5, as its atmospheric component). They found that the simulated GFS climatology was of comparable or higher quality to those with CESM1, except for cloud cover and radiative properties. The GFS-simulated global shortwave and longwave cloud radiative effects were only about half as large as observed, with profound effects on the simulated planetary energy budget. Xiao et al. (2014) found that much of this response was attributable to inadequate cloud cover over most parts of the oceans, including the near-coastal part of the subtropical stratocumulus regions and tropical-subtropical shallow cumulus regions. On the other hand, one of the few regions in which cloud

GMDD
7, 2249–2291, 2014

cover and radiative effects were overestimated in GFS is in the stratocumulus to cumulus transition regions, especially the East Pacific between the equator and 30° S. Thus, by focusing on the simulation of boundary layer clouds in the eastern subtropical oceans, we also hope to improve GFS-simulated cloud climatology in many other regions as well as globally averaged cloud radiative properties.

One focal strategy of the CPT is to use benchmark single-column model tests to identify possible model improvements, which are then tested in short global integrations. This paper describes some initial efforts to implement this strategy for improving GFS cloud simulations.

2 Method

We use GFS version 11.0.6 for both single column and global model experiments. The GFS single column model (SCM) used in this study, as well as the forcing files, can be downloaded at http://www.atmos.washington.edu/~jkf/GFS_SCM.html, which also includes instructions for running the SCM as well as routines modified for the experiments described in this paper. The global model may be downloaded at http://www.nco.ncep.noaa.gov/pmb/codes/nwprod/sorc/global_fcst.fd/.

2.1 Single column modelling

The SCM has proven a useful tool in testing general circulation model (GCM) physics on properties like clouds and precipitation in isolation from the effects of large-scale circulations (Randall et al., 2003). GCM developers can use SCMs to compare model performance to that of high resolution models such as large eddy simulation (LES) by running both with the same set of observationally-derived forcings. These forcings specify the initial thermodynamic and wind profiles, the tendencies of these profiles over the course of the simulation, and either the sea surface temperature or the surface latent and sensible heat fluxes. As part of the GEWEX Cloud System Study (GCSS, now

GMDD
7, 2249–2291, 2014

subsumed into the Global Atmospheric System Study or GASS), a rich set of forcing cases exists for this purpose, drawn from observational field campaigns encompassing different environments ranging from nocturnal marine stratocumulus to continental deep convection (e.g. Siebesma et al., 2003; Stevens et al., 2005; Grabowski et al., 2006).

The GFS has seldom been subject to this type of testing in the past, with developers generally focusing on global model skill scores based on errors of meteorological variables such as 500 hPa heights. Investigations of GFS physics that have used the single column modelling approach have been oriented toward cirrus clouds and ice phase microphysics (e.g. Luo et al., 2005). In single-column mode, we compare quantities relevant to the physics of warm boundary layer clouds, such as cumulus updraught mass flux and thermodynamic properties, to those of identically forced LES, using observationally-anchored cases. While single column modelling cannot substitute for sensitivity tests using 3-D simulations, this method's relative simplicity and comparability with LES makes it a useful tool for falsifying model physics and as a reference to guide interpretation of global model results.

Our approach thus far in using SCM to improve model physics has been to identify components of the parametrisations most relevant to boundary layer clouds that are (a) formulated in ways that are inconsistent with current knowledge of the process in question and (b) possible sources of model bias. We then aim to improve the component of the scheme while maintaining the general framework of the parametrisation. In other words, while, for example, the "dual mass flux" scheme of Neggers et al. (2009) is an attractive framework for unified parametrisation of large boundary layer eddies and shallow convection, to implement this in the GFS would require a complete overhaul of both the boundary layer and shallow convective schemes. Maintaining and improving the current framework is a more pragmatic approach to improving GFS physics in the short term. In some cases, sensitivity experiments comparing SCM to LES can identify sources of compensating errors, in which case simultaneous improvements must be made to several aspects of the physical parametrisations to reduce simulation biases.

GMDD
7, 2249–2291, 2014

The LES runs we compare to the SCM in this study use version 6 of the System for Atmospheric Modeling (SAM, Khairoutdinov and Randall, 2003). In all runs, SAM resolves the largest boundary layer eddies and all clouds, while smaller scale turbulence and microphysics are parametrised. SAM has been included in LES intercomparison studies for the GCSS cases used here (Siebesma et al., 2003; Stevens et al., 2005) and has been shown to reproduce observed precipitation, liquid water path, surface fluxes, and cloud fraction (where such observations are available) in those cases, except where we note otherwise.

2.2 Global model experiments

We also ran global model tests that complement our SCM experiments. Because global coupled model experiments are far more computationally expensive than single column experiments, we performed only three global experiments, with parameter changes chosen based partially on SCM results and partially on simultaneous development strategies at NCEP.

As in Xiao et al. (2014), we use the NCAR Atmospheric Modeling Work Group/Working Group on Numerical Experimentation diagnostic package (http://www.cgd.ucar.edu/amp/amwg/diagnostics) to facilitate comparison of our global model experiments with observations.

3 Model overview

This study is based on the 2011 version of GFS, the same as that used in the single column model. It has a spectral triangular truncation of 126 waves (T126), equivalent to roughly one degree horizontal grid spacing, and 64 hybrid sigma pressure levels (Sela, 2009). Compared with the previous version of the GFS, the main changes are in the parametrisations of the shallow convection, the planetary boundary layer (PBL),

GMDD
7, 2249–2291, 2014

and deep convection (Han and Pan, 2011). Features of these schemes are described in more detail in the next section.

This version of GFS uses the Atmospheric and Environmental Research Inc. Rapid Radiative Transfer Model longwave parametrisation (Mlawer et al., 1997). The shortwave parametrisation is modified from the National Aeronautics and Space Administration (NASA) Goddard Space Flight Center solar radiation scheme (Hou et al., 2002; Chou et al., 1998). Both radiation schemes assume maximum random cloud overlap.

The microphysics scheme (Zhao and Carr, 1997; Moorthi et al., 2001) prognoses cloud water specific humidity and cloud fraction following Sundqvist (1978). Both stratiform cloud processes and detrained cumulus cloud ice and condensate are sources of total cloud water.

For global simulations presented below, the GFS is coupled to the Modular Ocean Model 4 (MOM4), a finite difference version of the ocean primitive equations (Griffies et al., 2005). The zonal resolution is $1/2^\circ$. The meridional resolution gradually decreases from $1/4^\circ$ near the equator to $1/2^\circ$ at high latitudes. There are 40 height layers, whose vertical spacing increases from 10 m near the surface to about 500 m in the bottom.

4 Physics parametrisations

This section summarizes the GFS shallow convection, planetary boundary layer, and cloud fraction parametrisations, focusing on aspects relevant to our sensitivity tests. More detailed descriptions of these schemes are given by Troen and Mahrt (1986), Hong and Pan (1996) and Han and Pan (2011).

4.1 Shallow convection

The GFS shallow cumulus scheme (Han and Pan, 2011) is a bulk entraining plume mass flux parametrisation based on the GFS deep convection scheme (Pan and Wu,

GMDD
7, 2249–2291, 2014

1995; Han and Pan, 2011), but with new formulations of lateral entrainment and detrainment rate, a different mass-flux closure, and different plume microphysics.

The bulk plume originates from and shares the properties of the level of highest moist static energy in the boundary layer, usually the lowest model level. It rises to its lifted condensation level, where its mass flux is determined using the Grant (Grant and Brown, 1999) closure. The plume mass flux m is given by the equation

$$\frac{1}{m}\frac{\mathrm{d}m}{\mathrm{d}z} = \epsilon - \delta, \tag{1}$$

where ϵ is the fractional lateral entrainment rate and δ the fractional detrainment rate. The former is assumed to have the form $\epsilon = c/z$, where c is an adjustable nondimensional constant. The fractional detrainment rate δ is constant with height and equal to the fractional entrainment rate at the height of cloud base. This ensures a mass flux profile that decreases with height within the cumulus updraft, consistent with the LES study of Siebesma and Cuijpers (1995). It also means that changes to c affect the detrainment rate as well as the entrainment rate. The same entrainment rate is used in determining the moist static energy and total water specific humidity (and hence the buoyancy) of the cumulus updraught, as well as its horizontal velocity, relevant for cumulus momentum transport.

The bulk plume microphysics are simple: updraught liquid water is converted to precipitation (which falls down through the plume and can evaporate in the subcloud layer), and it is detrained to grid scale cloud condensate, both at rates proportional to the updraught liquid water content, following Lord (1978):

$$q_c^{\mathrm{prec}} \propto c_0 q_c^{\mathrm{cu}} \tag{2}$$

and

$$q_c^{\mathrm{detr}} \propto c_1 q_c^{\mathrm{cu}}. \tag{3}$$

The scheme contains a flag that turns off shallow convection if the cloud top (constrained to a model level) is below the model-diagnosed PBL top, diagnosed with a bulk

GMDD
7, 2249–2291, 2014

Richardson number. This ensures that clouds that lack the buoyancy to penetrate the inversion are handled entirely by the PBL scheme rather than the shallow convection scheme. In the operational GFS, this flag is commented out because it has little impact on NCEP's traditional forecast skill metrics. Our tests, discussed below, showed that this may nevertheless often be important to the parametrised boundary-layer cloud cover and precipitation.

Shallow cumulus cloud top is determined by cloud work function (Arakawa and Schubert, 1974), i.e. the vertically integrated buoyancy of the entraining updraught. Updraughts are given energy equal to 10 % of cloud work function to overshoot their level of neutral buoyancy. We test an alternative formulation of cloud top that instead uses an equation for the square of the cumulus updraught vertical velocity w:

$$\frac{1}{2}\frac{\mathrm{d}(w^2)}{\mathrm{d}z} = aB - b\epsilon w^2, \tag{4}$$

where a and b are tunable parameters and B is the cumulus updraught buoyancy. Choosing the parameters such that $b/a > 1$ roughly parametrises the effect of perturbation pressure gradients on vertical velocity (Bretherton et al., 2004).

Key parameters in the shallow convection scheme that affect its performance include the fractional entrainment/detrainment parameter c used in Eq. (1) and the rates c_0 and c_1 in Eqs. (2) and (3), respectively. If Eq. (4) is used to determine cloud top, then a and b may also be important parameters.

4.2 PBL turbulence and stratiform clouds

The GFS boundary layer turbulence parametrisation (Hong and Pan, 1996) is an eddy diffusivity scheme modified from Troen and Mahrt (1986) with an added "countergradient" term (for temperature only) representing the nonlocal mixing done by the largest PBL eddies. Han and Pan (2011) modified the turbulence scheme by adding a simple parametrisation of cloud top-driven mixing after Lock et al. (2000). This entrainment rate is proportional to the radiative flux jump across cloud top and represents cloud

GMDD
7, 2249–2291, 2014

top cooling enhancement of boundary layer entrainment. The original Lock scheme also parametrised mixing-induced buoyancy reversal; this process is not included in the GFS scheme.

The operational GFS uses two different cloud fraction schemes: one for radiative flux calculations, the other for stratiform microphysics calculations. The radiation scheme uses the Xu and Randall (1996) fit of observed cloud fraction to relative humidity RH, condensate specific humidity q_l, and saturation specific humidity q_s:

$$\sigma_{XR} = RH^{k_1}\left(1 - \exp\left\{-\frac{k_2 q_l}{[(1-RH)q_s]^{k_3}}\right\}\right). \quad (5)$$

The model uses the original Xu and Randall (1996) empirical values for the fit parameters: $k_1 = 0.25$, $k_2 = 100$, $k_3 = 0.49$. However, the condensate specific humidity used is only that of the stratiform microphysics scheme. Thus, cumulus convection only interacts with radiation indirectly through its effect on large-scale temperature and moisture fields. The stratiform microphysics scheme is derived from Sundqvist (1978) and parametrises cloud fraction based on relative humidity in excess of a prescribed, latitudinally-varying critical RH. CPT members at NCEP are developing a single cloud fraction scheme to be used throughout the model in future GFS versions.

5 Single column results

5.1 Model setup

The SCM is based on the operational version of the GFS, including the same 64 vertical levels, with vertical spacing in the PBL of 50–100 m. We run the SCM with a five-minute time step (half that used in the global simulations we present later in this paper), but the radiation scheme is called once per hour as in the GFS. In single column mode, horizontal tendencies in wind, temperature, and moisture fields are prescribed by the

GMDD
7, 2249–2291, 2014

forcing file in place of large-scale dynamics. The winds at each level are also forced by Coriolis and pressure-gradient forces, taking the initial wind profile as the geostrophic wind. The SCM's physical parametrisations are identical to those of the operational GFS except for options to include a few minor modifications planned for future GFS versions. These are discussed below and evaluated in our sensitivity experiments. Our single column sensitivity tests use two GCSS cases, described below.

5.2 BOMEX

For sensitivity tests to changing parameters in the shallow convection scheme, we utilize a nonprecipitating quasi-steady oceanic shallow cumulus case presented by Siebesma et al. (2003), derived from the Barbados Oceanographic and Meteorological Experiment (BOMEX, Holland and Rasmusson, 1973). The specified forcings already include the effects of radiative cooling, and cloud-radiation interaction is not considered in this case, so the radiation schemes are turned off in the SCM and the LES.

5.2.1 Experiment description

We use the BOMEX case to study model sensitivity to changing aspects of the shallow convection scheme. In accordance with the discussion in Sect. 3b, we test model sensitivity to changing several parameters. These parameter changes are summarized on Table 1. First, in the *ShCuCldCover* experiment, we include cumulus updraught condensate in the cloud fraction parametrization (Eq. 5). This change is included in subsequent experiments as well.

Second, we test sensitivity to the updraught lateral entrainment rate, parametrised as $\epsilon = c/z$. We run experiments with LES-compatible choices of c in the range of 1.0–2.0 (Siebesma et al., 2003) instead of the operational value $c = 0.3$. Because the GFS parametrises updraught detrainment rate as constant with height and equal to the entrainment rate at cloud base (where it is maximum within the cloud), changing c

GMDD
7, 2249–2291, 2014

also changes the detrainment rate. For this reason, we will henceforth refer to c as the entrainment/detrainment parameter.

At the same time, we test sensitivity to the efficiency of conversion of updraught condensate into precipitation or detrained condensate. The operational GFS converts updraught condensate in a grid layer to precipitation and detrains it to grid scale condensate at rates given in Eqs. (2) and (3); both rates are proportional to the condensate mixing ratio. This means that any updraught condensate is precipitated out over an e-folding depth of 400 m, causing extremely efficient precipitation even from the shallowest cumulus clouds. In practice, this compensates for the inadequate dilution of updraught condensate by lateral mixing, as we describe further below. In configuration *NewEntr*, we decreased these rates – in combination with increases to entrainment – to $c_0 = 0.001\,\mathrm{m}^{-1}$, $c_1 = 2.5 \times 10^{-4}\,\mathrm{m}^{-1}$. This can be regarded as an intermediate step toward the LES results: in *NewEntr* the lateral entrainment rate is still underestimated, compensated by overestimation of conversion of updraught condensation to precipitation, but both compensating errors are much smaller than with the operational parameter choices.

Lastly, we also show the effect of using the vertical velocity Eq. (4) to determine cloud top. We show the effect of this change both without the *NewEntr* change (*VvelOrig*) and with it (*VvelNewEntr*).

5.2.2 Results

Our initial sensitivity tests only involved single parameter changes. This quickly uncovered compensating errors – multiple parameters incorrectly tuned such that their effects cancel each other – in the shallow cumulus scheme. For example, only increasing the updraught lateral entrainment rate resulted in a simulation with an improved mass flux profile but far too small updraught condensate amount, while only decreasing the precipitation and detrainment conversion rates reduced excess precipitation but produced too much condensate. Furthermore, only reducing one of c_0 or c_1 simply shifted precipitation between the shallow convection and stratiform microphysics schemes, with

GMDD
7, 2249–2291, 2014

little reduction in overall precipitation. It is necessary to change all of these parameters together in order to address these compensating errors, so we only show results from simulations in which multiple parameters were changed.

Figure 1 shows profiles of liquid water potential temperature and total water specific humidity averaged over hours 3–6 of the BOMEX experiments. We show these primarily to give the reader a sense of the environment being simulated: a fairly well-mixed subcloud layer up to about 500 m, a conditionally unstable cloud layer, and a capping inversion starting slightly above 1400 m. SCM results differ from LES primarily in a less well-mixed subcloud layer, a more stably stratified cloud layer, and excess moisture at the inversion. This last feature is explored more in the forthcoming discussion. Biases are most extreme in the *VvelOrig* configuration, with profiles that imply far too much mixing with the free troposphere.

A major problem with the control GFS simulation of the BOMEX case is that it overprecipitates. The BOMEX case is idealized, but it is designed to mimic a several-day period during which observers and photographs suggest precipitation was negligible (Siebesma and Cuijpers, 1995), consistent with our LES results. Figure 2a shows time series of surface precipitation for the experiments. The control configuration maintains a convective precipitation rate of 1.5 mm day^{-1}, large enough to be a sizeable moisture sink to the trade cumulus boundary layer, compensating roughly 30 % of the surface evaporation. *NewEntr* reduces the convective precipitation by 60 %, but does not eliminate the problem because the precipitation flux is still proportional to the updraught condensate specific humidity, ensuring that all shallow convection will precipitate at least a little.

The *VvelOrig* configuration actually worsens the bias. Later we show that this is due to an overdeepening of cumulus convection. However, in combination with *NewEntr*, the spurious precipitation is reduced and the shallow convection scheme is prevented from switching off and on as it does in the non-*Vvel* experiments.

Figure 2 shows that all configurations maintain very small liquid water path for the first few hours of simulation. This is because nearly all the cloud water is associated

GMDD
7, 2249–2291, 2014

with the shallow convection scheme. At varying times in the simulation, however, the LWP raidly increases in the *Control*, *ShCuCldCover*, and *NewEntr* experiments. This indicates rapid development of stratiform cloud, which only the *Vvel* change is able to prevent.

Figure 3 shows profiles of stratiform cloud water and cloud fraction from both the stratiform microphysics scheme and the radiation scheme. In the left panel, we see that most of the stratiform condensation responsible for the rise in LWP in Fig. 2b occurs at one model level near cloud top. The reasons for this will be explored below. The right panel shows that simply adding cumulus condensate to the radiation cloud fraction – the *ShCuCldCover* change – is a major improvement, though the bias is now too much cloud cover rather than too little. This bias is reduced by subsequent parameter changes, and the spike in upper PBL cloud cover (and condensate) is removed by the *Vvel* change. Finally, comparing the middle and right panels shows the large difference that can exist between cloud fraction in the microphysics scheme and that of the radiation scheme.

Figure 4 shows time-averaged cumulus updraught properties: mass flux and condensate specific humidity. For the LES comparison, we define cumulus updraught properties as the average across all LES grid points that are both saturated and have positive vertical velocity.

The mass flux profiles of the *Control* and *ShCuCldCover* configurations show the effect of those experiments' high precipitation. Evaporation of rainfall below cloud base overstabilizes the subcloud layer, reducing cumulus updraught buoyancy such that convection is oftentimes only one or two grid levels deep – if it is not shut off completely. This leads to a time-averaged mass flux profile that is too bottom-heavy and biased low, particularly between 800 and 1200 m. However, the cloud top is in good agreement with LES.

The *NewEntr* parameter change improves on this by reducing precipitation directly (via the precipitation efficiency c_0) and indirectly (via increased entrainment dilution and reduced mass flux in the upper cloud layer). However, the cloud top is lower than

GMDD
7, 2249–2291, 2014

the *Control* configuration and LES – this is also due to increased entrainment dilution. The tendency of the GFS to produce too-low shallow cumulus cloud top when the entrainment rate is set to a value suggested by current knowledge is in fact why the operational value of c is so small.

The *Vvel* parameter change increases cloud depth and enhances penetrative entrainment of warm dry inversion air. This is what prevents stratiform condensation in the *Vvel* runs. With the operational settings for c, c_0, and c_1, the bias is over-corrected, with cloud top that is far too high. However, in combination with the *NewEntr* change, substantial improvement in the mass flux profile – as well as those shown in previous figures – is seen.

Finally, the right panel of Fig. 4 demonstrates the compensating errors at work in the shallow convection scheme. All configurations produce similar values for cumulus updraught condensate specific humidity, values that are close to that of LES. They do so via different tradeoffs between precipitation and entrainment. A major aspect of our parameter changes has aimed to shift the removal of updraught liquid water content away from precipitation and toward increased mixing with the free troposphere.

5.3 DYCOMS

To study model behavior in a stratocumulus environment, we use a case distilled from the Dynamics and Chemistry of Marine Stratocumulus (DYCOMS-II, referred to hereafter as DYCOMS) Research Flight 1, which sampled a nocturnal, nonprecipitating, well-mixed marine stratocumulus boundary layer under a strong capping inversion in the Northeast Pacific (Stevens et al., 2003). We use the GCSS DYCOMS case forcings as presented by Stevens et al. (2005) and Zhu et al. (2005). However, those studies used an idealized longwave radiation code in their simulations; we use the full model (longwave only) radiation code in both SCM and LES.

GMDD
7, 2249–2291, 2014

5.3.1 Experiment description

We found in our *Control* DYCOMS simulation that the shallow cumulus scheme was transporting much of the heat and moisture through the PBL despite this being a stratocumulus case (not shown). Recall from Sect. 3b that there is a logical flag within the shallow convection scheme code that turns shallow convection off if the cumulus cloud top is at or below PBL top. Thus, in boundary layers where moist updraughts have insufficient energy to penetrate the capping inversion, PBL cloudiness and entrainment will be handled by the PBL scheme rather than the cumulus convection scheme. This flag is not used by default, even though it is physically reasonable, but we experimented with using it, effectively turning convection off for the duration of the run. This "ShCu-Flag" experiment is shown along with the configurations already shown for the BOMEX case. The exception to this is the *ShCuCldCover* configuration, which has no effect on the DYCOMS case and is not shown here.

The operational GFS also includes a minimum background diffusion applied both in and above the PBL. The background diffusivity for heat and moisture in the operational GFS decreases exponentially with height from $1.0\,m^2\,s^{-1}$, giving rise to about $0.9\,m^2\,s^{-1}$ at the 900 hPa level, a typical PBL top in marine stratocumulus. To reduce erosion of coastal stratocumulus, NCEP developers have further reduced the lower inversion layers' background diffusivity; it is now 30 % of that at the surface (i.e. $0.3\,m^2\,s^{-1}$; Han and Pan, 2011). Hence, we use this reduced background diffusivity in our DYCOMS simulations.

5.3.2 Results

All DYCOMS experiments with the GFS maintain a reasonably strong capping inversion, given the model resolution, and produce cloud fraction of about 1.0 after initial spinup (not shown). In this respect, the DYCOMS SCM simulations do not have the same biases that the global coupled model shows in the Northeast Pacific, where the

GMDD
7, 2249–2291, 2014

model generates too shallow boundary layer and too low cloud fraction. This limits the interpretation of SCM results.

Figure 5 shows the evolution of precipitation and LWP. As noted by Stevens et al. (2005), LES models tend to underestimate LWP in the DYCOMS case, which was observed to be about 60 $g\,m^{-2}$. The SCM LWP is actually closer to observations. However, this is acheived with a drizzle rate of roughly 0.5 $mm\,d^{-1}$. Both observations (Stevens et al., 2003) and LES indicated no drizzle at the surface or even at cloud base. Thus it appears that, as with the convection scheme, the physics parametrisations controlling stratocumulus are too tuned toward precipitation as a mechanism for PBL drying. The simplest explanation is that the modified Lock et al. (2000) parametrisation in the SCM is not producing enough cloud top entrainment of warm, dry air. Initial results, to be reported in a future study, indicate that increasing the entrainment rate in the Lock scheme while simultaneously decreasing the autoconversion rate in the stratiform microphysics scheme can maintain observed LWP while reducing excess precipitation in the DYCOMS simulation.

The most obvious differences are between (1) the *Control* and *NewEntr* experiments, and (2) the *ShCuFlag* and *Vvel* experiments. As part of the implementation of using vertical velocity for cloud top prediction, a logical flag turning off shallow convection if it is less than 70 hPa deep is included. Thus, the *Vvel* configurations look just like the *ShCuFlag* configuration because all of them result in the model turning off shallow convection. Figure 5 shows that, without shallow convection, the model takes 2.5 h to spin up cloud LWP despite having a five-minute time step and having been initialized with a supersaturated moisture profile. However, experiments with a different stratocumulus case (not shown) show that this is not the case if the model is initialized with liquid water, and furthermore initializing with liquid water eliminates the oscillations that are seen when the shallow convection scheme is active.

GMDD
7, 2249–2291, 2014

6 Global model results

6.1 Configuration and experiment description

We perform four simulations with the global version of GFS coupled to MOM4: a 50 year run with GFS operational settings; a one year control run that, apart from length, is identical to the 50 year run; and two one year sensitivity experiments: shortrun1 and shortrun2. *Shortrun1* includes most of the parameter changes to the shallow convection scheme suggested by our BOMEX SCM study. *Shortrun2* also includes changes suggested by the DYCOMS study and by basic physical considerations not exposed by either SCM case. All experiments are identically initialized on 1 January 1948. The atmosphere is initialized by NCEP-NCAR reanalysis (Kalnay et al., 1996); the ocean is initialized with the Climate Forecast System Reanalysis (Saha et al., 2010), and the initial state is neutral with respect to the NINO3.4 (El Nino/Southern Oscillation) index. We included ocean-coupling for two reasons. First, it corresponds to the setup for seasonal climate prediction, an important application of GFS. Second, it was easier for us to set up a coupled simulation than an uncoupled simulation with seasonally varying SSTs.

The parameter changes in *Shortrun1* and *Shortrun2* are summarized in Table 2. *Shortrun1* increases the lateral entrainment rate and reduces the rain conversion rate in the shallow convection parametrisation, following two of the three prescriptions in the BOMEX *NewEntr* case. *Shortrun2* also reduces the condensate detrainment rate (the other parameter change made in *NewEntr*), uses cumulus condensate for cloud fraction, and uses the vertical velocity Eq. (4) for cloud top. *Shortrun2* also incorporates the additional changes discussed in the DYCOMS ShCuFlag case: to prevent shallow convection with a cloud top that does not extend above the PBL top and to decrease background diffusion in inversion layers. However, the former might have little impact in combination with the vertical velocity cloud top change, as was seen in the DYCOMS simulations.

GMDD
7, 2249–2291, 2014

For physical correctness, a parametrisation of heating due to turbulent kinetic energy (TKE) dissipation is included. We expect this to have negligible impact on any SCM simulation of existing subtropical boundary layer cloud cases. Viscous dissipation of TKE can be a significant source of heat, especially in strong wind conditions such as in hurricanes (Bister and Emanuel, 1998). Although not shown in this paper, inclusion of TKE dissipative heating not only increased the 10 m maximum wind about 10–30 % in hurricane forecasts, but also largely reduced the unexplained GFS atmospheric energy loss of about 4–5 $W m^{-2}$. These results will be presented in a forthcoming paper; they have little effect on subtropical boundary layer clouds.

For the following discussion we focus on marine low cloud sensitivity in the southeastern Pacific for September–October–November (SON). Even though this is only 9–11 months after the start of the simulations, the climatological marine low cloud bias and its sensitivity to parameter changes has already emerged, as can be seen by comparing Fig. 6a (the one year run) and d (the 50 year run). Cloudiness differences driven by synoptic timescale variability in the southeastern Pacific may affect the exact magnitudes of changes in the bias in the sensitivity experiments; by comparing the differences between the simulations in the three individual months comprising the SON period (not shown) we are confident that the signals we report are robust to synoptically-driven cloudiness fluctuations.

6.2 Results

Figures 6 and 7 show the sensitivity of shortwave cloud radiative effect (SWCRE) and low cloud fraction over the Pacific region for SON. In these plots, panel (a) shows the bias of the control simulation compared to satellite-derived climatologies, and the next two panels show the difference of the control from the two sensitivity runs. The observations used in Fig. 7a are a combination of the climatological low cloud fraction from the CLOUDSAT/CALIPSO GEOPROF product (Kay and Gettelman, 2009) and the CALIPSO GOCCP product (Chepfer et al., 2010) for 2006–2010 – in each grid box the maximum low cloud fraction from the two is used. This method enhances the

GMDD
7, 2249–2291, 2014

low cloud fraction just off the west coasts of the American and African continents because GEOPROF tends to underestimate low cloud amount because it screens out clouds with tops below 500 m altitude. However, GEOPROF is more accurate in general because the combination of CLOUDSAT and CALIPSO instruments can detect low clouds better when mid- and high-level clouds are present. The SWCRE observation used in Fig. 6a and d is from the Clouds and Earth's Radiant Energy System Edition 2 (CERES2, Minnis et al., 2011) for 2000–2005. In these panels, biases on the *Control* simulation are reduced where the colours indicate differences of the same sign as the upper panel (e.g. blue colours where there is a blue colour in the upper panel, or vice versa).

In the southeastern Pacific, *Control* shows large positive errors of SWCRE (Fig. 6a) near the South American coast and negative errors further offshore, which corresponds clearly to the errors in marine low clouds (Fig. 7a), as discussed in Xiao et al. (2014). *Shortrun1* (Figs. 6b and 7b) shows small but consistent reduction of errors in low cloud fraction (less than 10 %) and SWCRE (less than 10 $W m^{-2}$) both near the South American coast and in the open ocean, while *Shortrun2* shows similar patterns of error reduction but with much larger amplitude – 20–30 $W m^{-2}$ for SWCRE. In the tropics (15° S–15° N), the overextension of low clouds onto the equator from the southeastern Pacific is also reduced in *Shortrun2*. There is also a large reduction of SWCRE errors in the Inter-Tropical Convergence Zone (ITCZ) and South Pacific Convergence Zone (SPCZ) in *Shortrun2*, which we will discuss in more detail together with the SST response later in this section. The global mean SWCRE bias in *Shortrun2*, compared to that in *Control*, is reduced by about half, from 23 to 11 $W m^{-2}$ for the annual average of 1948 minus the CERES2 annual mean from 2000–2005; this bias reduction occurs persistently throughout the year.

Figure 8 shows the sensitivity of low cloud structure along 20° S in the East and Central Pacific for SON. In *Control* (Fig. 8b), the lack of clouds near the coast and the overextension offshore is clear in comparison to the

GMDD
7, 2249–2291, 2014

CERES2-MODIS-CALIPSO-CLOUDSAT (CCCM) dataset from the Atmospheric Science Data Center at NASA Langley Research Center (Fig. 8a).

In *Shortrun1* (Fig. 8c), the stratocumulus layer gets slightly thinner in general but the maximum in cloud water content increases and remains too far offshore, making the total error reduction small. This is likely because decreasing the shallow cumulus precipitation efficiency c_0 without changing the condensate detrainment rate c_1 simply shifts the shallow convective condensate sink from precipitation to detrainment to grid scale cloud. *Shortrun2* (Fig. 8d), on the other hand, shows reduced cloud water content offshore and increased cloud water close to the coast, more consistent with observations. However, the cloud layer in *Shortrun2* extends too deep and the trade-wind inversion is weakened (not shown). Furthermore, both *Shortrun1* and *Shortrun2* show excessive cloud liquid water compared to CCCM in the trade cumulus regime extending across the westernmost part of the cross-section, worsening a bias already present in *control*.

The cloud structure changes can be related to changes in the behaviour of the parametrised shallow convection. Figure 9 shows heating and moistening from the shallow convection scheme in each experiment along the transect. The difference between *Shortrun2* and *Shortrun1* east of 100° W shows that nearly all shallow convective activity has been eliminated in this region, which is observed to be dominated by stratocumulus clouds. Meanwhile, increasing the entrainment/detrainment parameter (one of the two differences between *Shortrun1* and *Control*) decreases mass flux in the upper cloud layers and thus reduces convective heating in the cumulus and Sc–Cu transition regions west of 100° W.

The SST response in SON is shown in Fig. 10 for *Shortrun2*. The response in *Shortrun1* is small and not shown here. In *Control*, we see large positive SST errors near the American coasts (4 °C off South American coast) and negative biases to their west (−2 °C in the southeastern Pacific). In the tropics, there are warm SST biases of 2 °C along the ITCZ and SPCZ and near the maritime continent, and negative biases along the equator. In *Shortrun2*, the negative biases in the southeastern Pacific are reduced

GMDD
7, 2249–2291, 2014

by at least half but the warm biases near the coast are not reduced. In the tropics the warm biases along ITCZ and SPCZ and near the maritime continent are reduced, but the equatorial cold bias is turned into a warm bias, especially between 150–180° W. We attribute these SST changes to reduced cloud radiative forcing biases in the deep convective region (see Figs. 6 and 7) that, along with improvement to the boundary layer clouds, help weaken the Walker circulation, with feedbacks from associated precipitation changes. Such sensitivity of the basin-wide Hadley–Walker circulation pattern to changes in marine low clouds associated with parameter changes in shallow convection and moist turbulence parametrisation is also found in other GCMs (e.g. Ma et al., 1994; Xiao et al., 2014).

7 Data assimilation tests

In addition to the global coupled model tests, some of these changes have also been tested in data assimilation (DA) mode. Here we briefly present pertinent results from a global DA experiment. Apart from the parametrisations being tested, these are run with the operational GFS with T382 resolution. After two weeks of model spinup, we present the results of one week of 72 h forecasts. While this is shorter than a typical 2–3 month comparison, it shows cloud changes that are consistent with our climate runs, while also exposing other forecast biases that our changes appear to slightly worsen.

The two experiments shown here correspond to the SCM *Control* and *NewEntr* cases. Recall that the latter adds cumulus (shallow and deep) condensate to the radiation scheme's cloud fraction, increases shallow cumulus lateral entrainment, and reduces the condensate precipitation and detrainment efficiencies.

7.1 Results

Figure 11 shows that, compared to the operational GFS, the *NewEntr* change increases global low cloud fraction, with a global mean increase of 4 %. Substantial

GMDD
7, 2249–2291, 2014

increases are seen throughout tropical marine locations. It also increases the global top-of-atmosphere (TOA) upwelling shortwave radiation by 5 $W m^2$ and decreases TOA outgoing longwave radiation by 1 $W m^{-2}$. These are all reductions in biases.

However, as Fig. 12 shows, this change also increases the root mean square error in tropical (15° S–15° N) horizontal winds. Tropical wind RMSE increases for all forecasts in the lower atmosphere and through the depth of the troposphere for longer forecasts.

7.2 Implications

As a consequence of these experiments, further work must be done before these changes can be implemented into future versions of the GFS; climate improvements must, at the very least, have a neutral impact on forecasts. Single column tests (not shown) indicate that changes in horizontal winds are not a result of cumulus momentum transport – the *NewEntr* change has no impact on winds in the SCM. Instead, the change is affecting horizontal pressure gradients; thus more global model tests are needed to investigate this further.

8 Conclusions

The NOAA stratocumulus-to-cumulus transition Climate Process Team has run sensitivity experiments to single-column and global coupled versions of the NCEP-GFS model in conjunction. To improve the GFS simulation of subtropical boundary layer cloud, we used single-column simulations to identify and attribute underlying problems in the shallow convection scheme, and we then tested improvements suggested by this approach in short global coupled simulations.

In single-column mode, we found that some simple parameter changes to the shallow convection scheme improved simulated boundary-layer structure and precipitation compared to LES. In particular, it is beneficial to increase cumulus lateral mixing with the environment and decrease the rate at which updraught condensate falls out as rain

GMDD
7, 2249–2291, 2014

and is detrained to the grid scale. This shifts some of the cumulus updraught removal of water from precipitation to evaporation associated with entrainment.

However, the single-column model still over-precipitates in both shallow convective and stratiform environments. We hypothesize that this can be improved by increasing entrainment of warm, dry free-tropospheric air into the boundary layer through changes to the boundary layer scheme, by reducing autoconversion of liquid cloud water to rain in the stratiform microphysics scheme, and by reformulating shallow convective precipitation to supress all rainfall when condensate specific humidity is small.

One year global coupled model experiments combining these changes substantially reduce biases in subtropical low cloud fraction and shortwave cloud forcing seen in the control version of GFS. Improvements are seen in the deep convective regions as well as the subtropical boundary-layer cloud regimes. Global model changes also improve SST and precipitation bias in most regions. However, underestimation of low cloud off the subtropical west coasts of the Americas remains a problem even after the changes, and increased tropical wind RMSE must be addressed before this change can be implemented in the GFS.

The CPT's focus has been improving cloud regimes associated with the stratocumulus to trade cumulus transition. As we continue our GFS development efforts, we will take a more holistic approach, focusing on better simulation of global cloud cover and its radiative effects through improvements of the microphysics, cloud fraction, cumulus convection, and PBL parametrisations and their interactions.

Supplementary material related to this article is available online at http://www.geosci-model-dev-discuss.net/7/2249/2014/gmdd-7-2249-2014-supplement.zip.

Acknowledgements. This work is supported by NOAA MAPP grant GC10-670a as part of the Sc–Cu Climate Process Team. The first author would like to thank Hua-Lu Pan at NCEP for his support and Peter Blossey at University of Washington for providing LES runs.

GMDD
7, 2249–2291, 2014

References

Arakawa, A. and Schubert, W. H.: Interaction of a cumulus cloud ensemble with the large-scale environment, J. Atmos. Sci., 31, 674–701, doi:10.1175/1520-0469(1974)031<0674:ioacce>2.0.co;2, 1974. 2257

Bister, M. and Emanuel, K. A.: Dissipative heating and hurricane intensity, Meteorol. Atmos. Phys., 65, 233–240, 1998. 2267

Bretherton, C. S., McCaa, J. R., and Grenier, H.: A new parameterization for shallow cumulus convection and its application to marine subtropical cloud-topped boundary layers, Part I: Description and 1D results, Mon. Weather Rev., 132, 864–882, doi:10.1175/1520-0493(2004)132<0864:anpfsc>2.0.co;2, 2004. 2257

Chepfer, H., Bony, S., Winker, D., Cesana, G., Dufresne, J. L., Minnis, P., Stubenrauch, C. J., and Zeng, S.: The GCM-Oriented CALIPSO Cloud Product (CALIPSO-GOCCP), J. Geophys. Res.-Atmos., 115, 2156–2202, doi:10.1029/2009jd012251, 2010. 2267

Chou, M. D., Suarez, M. J., Ho, C. H., Yan, M. M. H., and Lee, K. T.: Parameterizations for cloud overlapping and shortwave single-scattering properties for use in general circulation and cloud ensemble models, J. Climate, 11, 202–214, doi:10.1175/1520-0442(1998)011<0202:pfcoas>2.0.co;2, 1998. 2255

Grabowski, W. W., Bechtold, P., Cheng, A., Forbes, R., Halliwell, C., Khairoutdinov, M., Lang, S., Nasuno, T., Petch, J., Tao, W. K., Wong, R., Wu, X., and Xu, K. M.: Daytime convective development over land: a model intercomparison based on LBA observations, Q. J. Roy. Meteorol. Soc., 132, 317–344, doi:10.1256/qj.04.147, 2006. 2253

Grant, A. L. M. and Brown, A. R.: A similarity hypothesis for shallow-cumulus transports, Q. J. Roy. Meteorol. Soc., 125, 1913–1936, doi:10.1256/smsqj.55801, 1999. 2256

Griffies, S. M., Gnanadesikan, A., Dixon, K. W., Dunne, J. P., Gerdes, R., Harrison, M. J., Rosati, A., Russell, J. L., Samuels, B. L., Spelman, M. J., Winton, M., and Zhang, R.: Formulation of an ocean model for global climate simulations, Ocean Sci., 1, 45–79, doi:10.5194/os-1-45-2005, 2005. 2255

Han, J. and Pan, H.-L.: Revision of convection and vertical diffusion schemes in the NCEP global forecast system, Weather Forecast., 26, 520–533, doi:10.1175/waf-d-10-05038.1, 2011. 2255, 2256, 2257, 2264

GMDD
7, 2249–2291, 2014

Holland, J. Z. and Rasmusson, E. M.: Measurements of atmospheric mass, energy, and momentum budgets over a 500-kilometer square of tropical ocean, Mon. Weather Rev., 101, 44–55, doi:10.1175/1520-0493(1973)101<0044:motame>2.3.co;2, 1973. 2259

Hong, S. Y. and Pan, H. L.: Nonlocal boundary layer vertical diffusion in a Medium-Range Forecast Model, Mon. Weather Rev., 124, 2322–2339, doi:10.1175/1520-0493(1996)124<2322:nblvdi>2.0.co;2, 1996. 2255, 2257

Hou, Y., Moorthi, S., and Compana, K.: Parameterization of solar radiation transfer in NCEP models, NCEP Office Note #441, available at: http://www.emc.ncep.noaa.gov/officenotes/FullTOC.html#2000 (last access: February 2014), 2002. 2255

Kalnay, E., Kanamitsu, M., Kistler, R., Collins, W., Deaven, D., Gandin, L., Iredell, M., Saha, S., White, G., Woollen, J., Zhu, Y., Chelliah, M., Ebisuzaki, W., Higgins, W., Janowiak, J., Mo, K. C., Ropelewski, C., Wang, J., Leetmaa, A., Reynolds, R., Jenne, R., and Joseph, D.: The NCEP/NCAR 40-year reanalysis project, B. Am. Meteorol. Soc., 77, 437–471, doi:10.1175/1520-0477(1996)077<0437:tnyrp>2.0.co;2, 1996. 2266

Kay, J. E. and Gettelman, A.: Cloud influence on and response to seasonal Arctic sea ice loss, J. Geophys. Res.-Atmos., 114, 2156–2202, doi:10.1029/2009JD011773, 2009. 2267

Khairoutdinov, M. F. and Randall, D. A.: Cloud resolving modeling of the ARM summer 1997 IOP: model formulation, results, uncertainties, and sensitivities, J. Atmos. Sci., 60, 607–625, doi:10.1175/1520-0469(2003)060<0607:crmota>2.0.co;2, 2003. 2254

Lock, A. P., Brown, A. R., Bush, M. R., Martin, G. M., and Smith, R. N. B.: A new boundary layer mixing scheme, Part I: Scheme description and single-column model tests, Mon. Weather Rev., 128, 3187–3199, doi:10.1175/1520-0493(2000)128<3187:anblms>2.0.co;2, 2000. 2257, 2265

Lord, S.: Development and observational verification of cumulus cloud parameterization, Ph.D. thesis, University of California, Los Angeles, 1978. 2256

Luo, Y. L., Krueger, S. K., and Moorthi, S.: Cloud properties simulated by a single-column model, Part I: Comparison to cloud radar observations of cirrus clouds, J. Atmos. Sci., 62, 1428–1445, doi:10.1175/jas3425.1, 2005. 2253

Ma, C. C., Mechoso, C. R., Arakawa, A., and Farrara, J. D.: Sensitivity of a coupled ocean-atmosphere model to physical parameterizations, J. Climate, 7, 1883–1896, doi:10.1175/1520-0442(1994)007<1883:soacom>2.0.co;2, 1994. 2270

GMDD
7, 2249–2291, 2014

Mlawer, E. J., Taubman, S. J., Brown, P. D., Iacono, M. J., and Clough, S. A.: Radiative transfer for inhomogeneous atmospheres: RRTM, a validated correlated-k model for the longwave, J. Geophys. Res.-Atmos., 102, 16663–16682, doi:10.1029/97jd00237, 1997. 2255

Moorthi, S., Pan, H.-L., and Caplan, P.: Changes to the 2001 NCEP operational MRF/AVN global analysis/forecast system, NWS Tech. Procedures Bulletin, 484, available at: http://www.nws.noaa.gov/om/tpb/484.htm (last access: February 2014), 2001. 2255

Neggers, R. A. J., Koehler, M., and Beljaars, A. C. M.: A dual mass flux framework for boundary layer convection, Part I: Transport, J. Atmos. Sci., 66, 1465–1487, doi:10.1175/2008jas2635.1, 2009. 2253

Pan, H. and Wu, W.: Implementing a mass flux convective parameterization package for the NMC Medium-Range Forecast model, NMC Office Note 409, available at: http://www.emc.ncep.noaa.gov/officenotes/FullTOCx.html#1990 (last access: February 2014), 1995. 2255

Randall, D., Krueger, S., Bretherton, C., Curry, J., Duynkerke, P., Moncrieff, M., Ryan, B., Starr, D., Miller, M., Rossow, W., Tselioudis, G., and Wielicki, B.: Confronting models with data – the GEWEX cloud systems study, B. Am. Meteorol. Soc., 84, 455–469, doi:10.1175/bams-84-4-455, 2003. 2252

Saha, S., Nadiga, S., Thiaw, C., Wang, J., Wang, W., Zhang, Q., Van den Dool, H. M., Pan, H. L., Moorthi, S., Behringer, D., Stokes, D., Pena, M., Lord, S., White, G., Ebisuzaki, W., Peng, P., and Xie, P.: The NCEP climate forecast system, J. Climate, 19, 3483–3517, doi:10.1175/jcli3812.1, 2006. 2251

Saha, S., Moorthi, S., Pan, H.-L., Wu, X., Wang, J., Nadiga, S., Tripp, P., Kistler, R., Woollen, J., Behringer, D., Liu, H., Stokes, D., Grumbine, R., Gayno, G., Wang, J., Hou, Y.-T., Chuang, H.-Y., Juang, H.-M. H., Sela, J., Iredell, M., Treadon, R., Kleist, D., Van Delst, P., Keyser, D., Derber, J., Ek, M., Meng, J., Wei, H., Yang, R., Lord, S., Van den Dool, H., Kumar, A., Wang, W., Long, C., Chelliah, M., Xue, Y., Huang, B., Schemm, J.-K., Ebisuzaki, W., Lin, R., Xie, P., Chen, M., Zhou, S., Higgins, W., Zou, C.-Z., Liu, Q., Chen, Y., Han, Y., Cucurull, L., Reynolds, R. W., Rutledge, G., and Goldberg, M.: The NCEP climate forecast system reanalysis, B. Am. Meteorol. Soc., 91, 1015–1057, doi:10.1175/2010bams3001.1, 2010. 2251, 2266

Sela, J.: Implementation of the sigma pressure hybrid coordinate into GFS, Tech. rep., NCEP Office Note 461, NCEP, http://www.lib.ncep.noaa.gov/ncepofficenotes/files/on461.pdf (last access: April 2014), 2009. 2254

GMDD
7, 2249–2291, 2014

Siebesma, A. P. and Cuijpers, J. W. M.: Evaluation of parametric assumptions for shallow cumulus convection, J. Atmos. Sci., 52, 650–666, doi:10.1175/1520-0469(1995)052<0650:eopafs>2.0.co;2, 1995. 2256, 2261

Siebesma, A. P., Bretherton, C. S., Brown, A., Chlond, A., Cuxart, J., Duynkerke, P. G., Jiang, H. L., Khairoutdinov, M., Lewellen, D., Moeng, C. H., Sanchez, E., Stevens, B., and Stevens, D. E.: A large eddy simulation intercomparison study of shallow cumulus convection, J. Atmos. Sci., 60, 1201–1219, doi:10.1175/1520-0469(2003)60<1201:alesis>2.0.co;2, 2003. 2253, 2254, 2259

Stevens, B., Lenschow, D. H., Vali, G., Gerber, H., Bandy, A., Blomquist, B., Brenguier, J. L., Bretherton, C. S., Burnet, F., Campos, T., Chai, S., Faloona, I., Friesen, D., Haimov, S., Laursen, K., Lilly, D. K., Loehrer, S. M., Malinowski, S. P., Morley, B., Petters, M. D., Rogers, D. C., Russell, L., Savic-Jovac, V., Snider, J. R., Straub, D., Szumowski, M. J., Takagi, H., Thornton, D. C., Tschudi, M., Twohy, C., Wetzel, M., and van Zanten, M. C.: Dynamics and chemistry of marine stratocumulus – DYCOMS-II, B. Am. Meteorol. Soc., 84, 579–593, doi:10.1175/bams-84-5-579, 2003. 2263, 2265

Stevens, B., Moeng, C. H., Ackerman, A. S., Bretherton, C. S., Chlond, A., De Roode, S., Edwards, J., Golaz, J. C., Jiang, H. L., Khairoutdinov, M., Kirkpatrick, M. P., Lewellen, D. C., Lock, A., Muller, F., Stevens, D. E., Whelan, E., and Zhu, P.: Evaluation of large-Eddy simulations via observations of nocturnal marine stratocumulus, Mon. Weather Rev., 133, 1443–1462, doi:10.1175/mwr2930.1, 2005. 2253, 2254, 2263

Sundqvist, H.: Parameterization scheme for non-convective condensation including prediction of cloud water content, Q. J. Roy. Meteorol. Soc., 104, 677–690, doi:10.1002/qj.49710444110, 1978. 2255, 2258

Troen, I. and Mahrt, L.: A simple model of the atmospheric boundary layer – sensitivity to surface evaporation, Bound.-Lay. Meteorol., 37, 129–148, doi:10.1007/bf00122760, 1986. 2255, 2257

Xiao, H., Mechoso, C. R., Sun, R., Han, J., Park, S., Hannay, S., Teixeira, J., and Bretherton, C.: Diagnosis of the marine low cloud simulation in the NCAR Community Earth System Model (CESM) and the NCEP Global Forecast System (GFS)-Modular Ocean Model v4 (MOM4) coupled model, Clim. Dynam., doi:10.1007/s00382-014-2067-y, in press, 2014. 2251, 2254, 2268, 2270

GMDD
7, 2249–2291, 2014

Xu, K. M. and Randall, D. A.: A semiempirical cloudiness parameterization for use in climate models, J. Atmos. Sci., 53, 3084–3102, doi:10.1175/1520-0469(1996)053<3084:ascpfu>2.0.co;2, 1996. 2258

Zhao, Q. Y. and Carr, F. H.: A prognostic cloud scheme for operational NWP models, Mon. Weather Rev., 125, 1931–1953, doi:10.1175/1520-0493(1997)125<1931:apcsfo>2.0.co;2, 1997. 2255

Zhu, P., Bretherton, C. S., Kohler, M., Cheng, A. N., Chlond, A., Geng, Q. Z., Austin, P., Golaz, J. C., Lenderink, G., Lock, A., and Stevens, B.: Intercomparison and interpretation of single-column model simulations of a nocturnal stratocumulus-topped marine boundary layer, Mon. Weather Rev., 133, 2741–2758, doi:10.1175/mwr2997.1, 2005. 2263

GMDD
7, 2249–2291, 2014

Table 1. Parameter settings for SCM experiments with the BOMEX shallow convection cases. Parameters *a* and *b* refer to coefficients in Eq. (4)

	Control	*ShCuCldCover*	*NewEntr*	*VvelOrig*	*VvelNewEntr*
ShCu cloud	No	Yes	Yes	Yes	Yes
c	0.3	0.3	1.0	0.3	1.0
c_0 [m^{-1}]	2.0×10^{-3}	2.0×10^{-3}	1.0×10^{-3}	2.0×10^{-3}	1.0×10^{-3}
c_1 [m^{-1}]	5.0×10^{-4}	5.0×10^{-4}	2.5×10^{-4}	5.0×10^{-4}	2.5×10^{-4}
a	NA	NA	NA	$\approx \frac{1}{3}$	$\approx \frac{1}{3}$
b	NA	NA	NA	≈ 6	≈ 6

GMDD
7, 2249–2291, 2014

Table 2. Parameter settings for free-running coupled global model experiments.

	Control	*Shortrun1*	*Shortrun2*
ShCu Cloud	No	No	Yes
c	0.3	1.0	1.0
c_0 [m^{-1}]	2.0×10^{-3}	1.0×10^{-3}	1.0×10^{-3}
c_1 [m^{-1}]	5.0×10^{-4}	5.0×10^{-4}	2.5×10^{-4}
a	NA	NA	$\approx \frac{1}{3}$
b	NA	NA	≈ 6
ShCu Depth Flag	No	No	Yes
PBL Bckgrnd Diff [$m^2\,s^{-1}$]	0.3	0.3	1.0
TKE Dissipative Heating	No	No	Yes

GMDD
7, 2249–2291, 2014

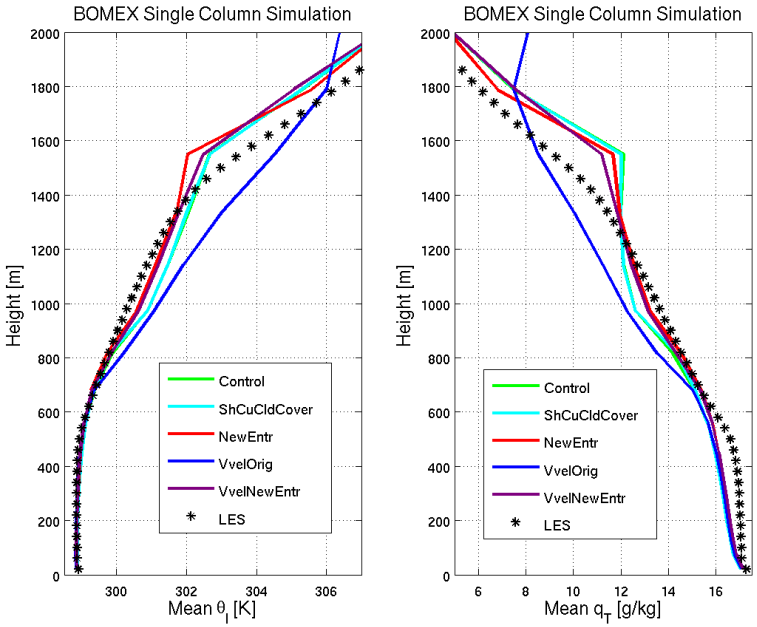

Fig. 1. BOMEX liquid water potential temperature (left panel) and total water (right panel) profiles averaged over hours 3–6. Coloured lines are different SCM experiments; black stars are LES.

GMDD
7, 2249–2291, 2014

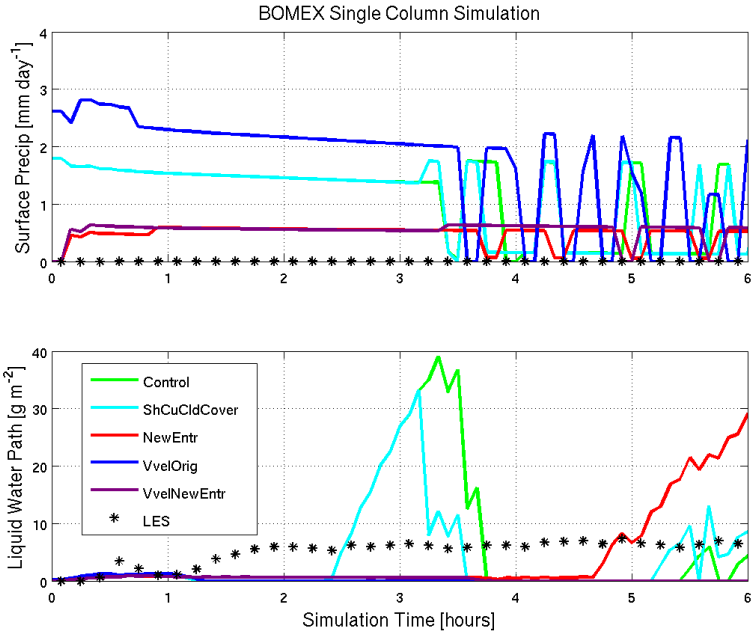

Fig. 2. BOMEX time series of surface precipitation rate (top panel) and liquid water path (bottom panel) in the first six hours of simulation. Coloured lines are different SCM experiments; black stars are LES.

GMDD
7, 2249–2291, 2014



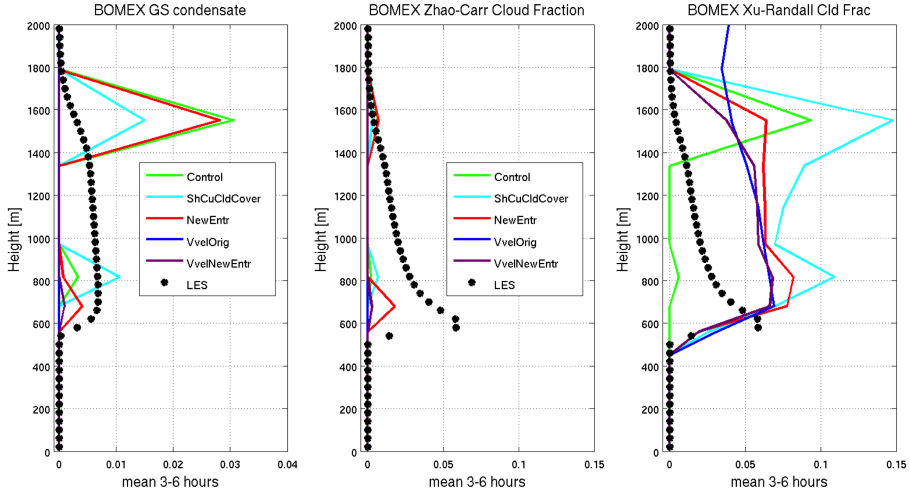

Fig. 3. BOMEX grid scale condensate (left panel, g kg^{-1}) and cloud fraction as calculated in the stratiform microphysics (centre panel) and radiation (right panel) parametrisations, averaged over hours 3–6. Coloured lines are different SCM experiments; black stars are LES.

GMDD
7, 2249–2291, 2014




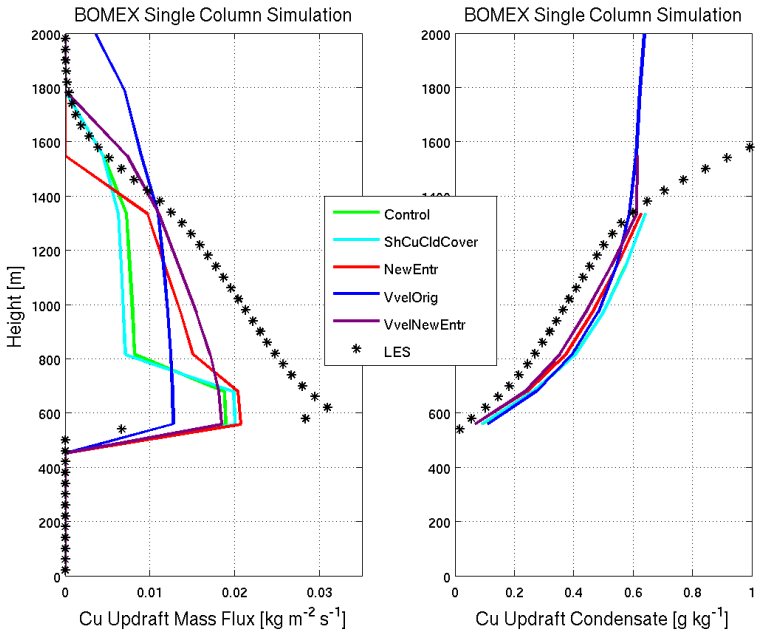

Fig. 4. BOMEX shallow cumulus updraught (left panel) mass flux and (right panel) condensate profiles averaged over hours 3–6. Coloured lines are different SCM experiments; black stars are LES.

GMDD
7, 2249–2291, 2014

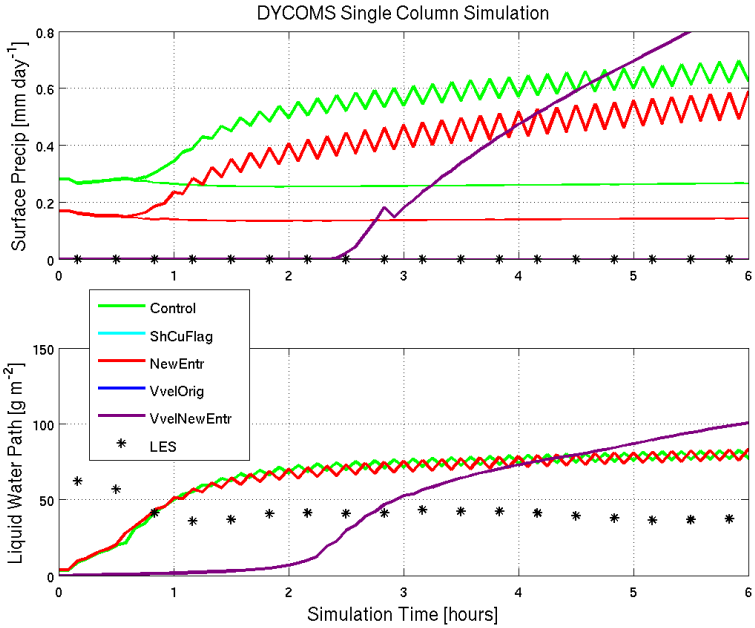

Fig. 5. DYCOMS time series of surface precipitation rate (top panel) and liquid water path (bottom panel) in the first six hours of simulation. Coloured lines are different SCM experiments; black stars are LES.

GMDD
7, 2249–2291, 2014

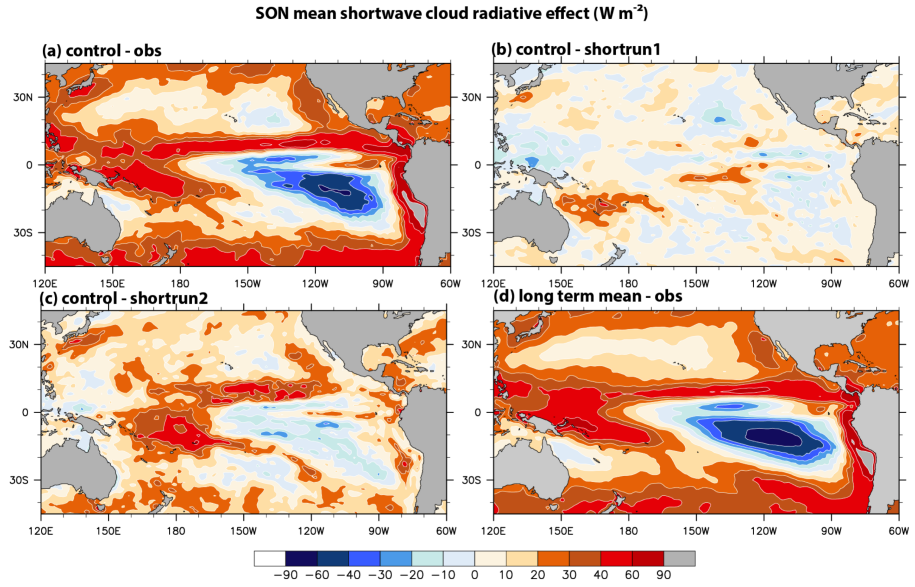

Fig. 6. Shortwave cloud forcing biases and their improvements in global simulations. **(a)** Shows the bias in the control run compared to observations; **(b)** shows the difference between *Control* and *Shortrun1*; **(c)** shows the difference between *Control* and *Shortrun2*. In **(b)** and **(c)**, the respective experiment bias has been eliminated to the extent that the pattern matches **(a)**. See text for further explanation. **(d)** Shows the bias in the 50 year control run.

GMDD
7, 2249–2291, 2014

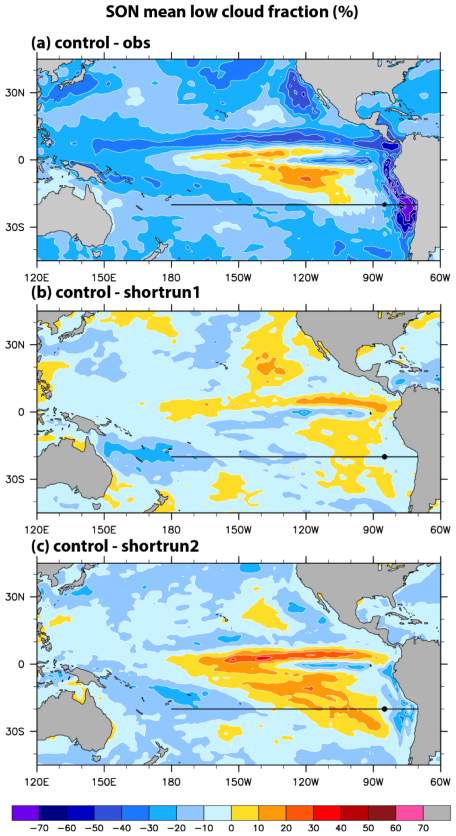

Fig. 7. Cloud fraction bias and its improvement in global simulations. **(a)** Shows the bias in the *Control* run compared to observations; **(b)** shows the difference between control and *Shortrun1*; **(c)** shows the difference between *Control* and *Shortrun2*. In **(b)** and **(c)**, the respective experiment bias has been eliminated to the extent that the pattern matches **(a)**. See text for further explanation.

GMDD
7, 2249–2291, 2014

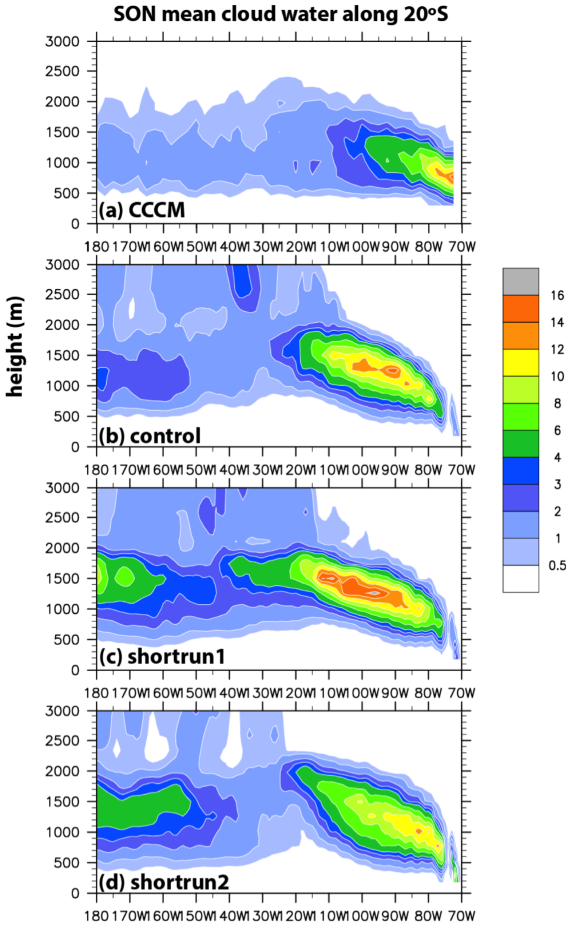

Fig. 8. Cloud condensate along the 20° S Pacific cross section in **(a)** observations; **(b)** the *Control* run; **(c)** *Shortrun1*, and **(d)** *Shortrun2*.

GMDD
7, 2249–2291, 2014

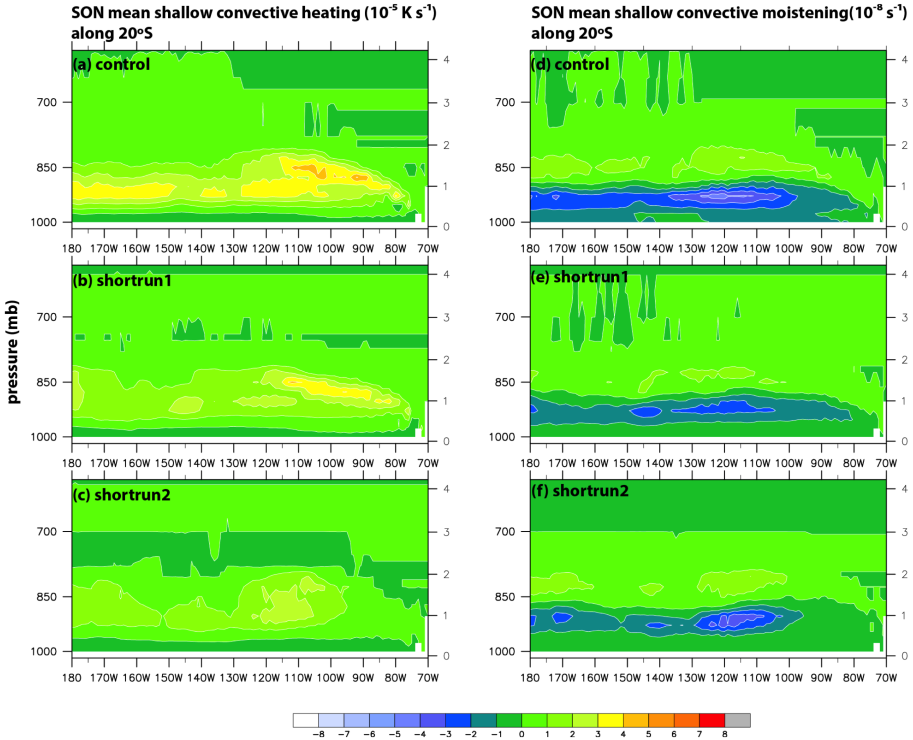

Fig. 9. Shallow cumulus heating (left column) and moistening (right column) in the *Control* run (top panels), *Shortrun1* (middle panels), and *Shortrun2* (bottom panels).

GMDD
7, 2249–2291, 2014

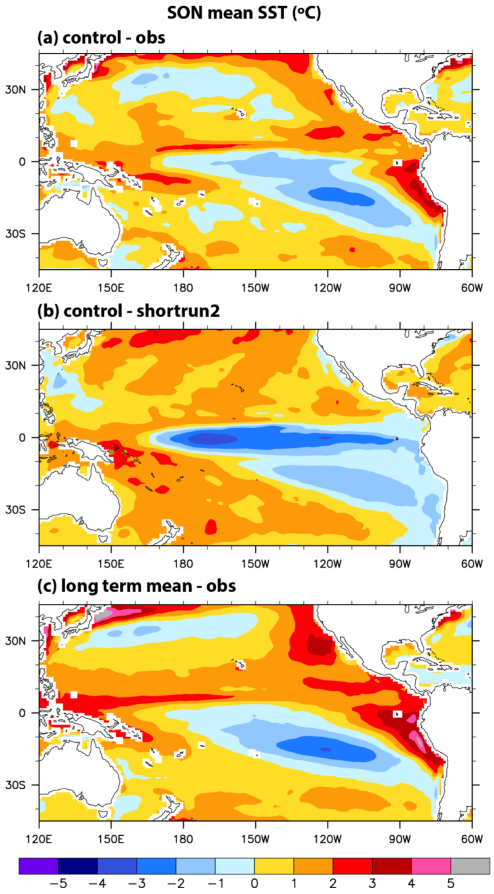

Fig. 10. Pacific SST in global simulations: **(a)** bias in the *Control* run; **(b)** the difference between *Control* and *Shortrun2*, and **(c)** bias in the 50 year *Control* run. In **(b)**, the experiment has eliminated the bias to the extent that the pattern matches that of **(a)**. See text for further explanation.

GMDD
7, 2249–2291, 2014

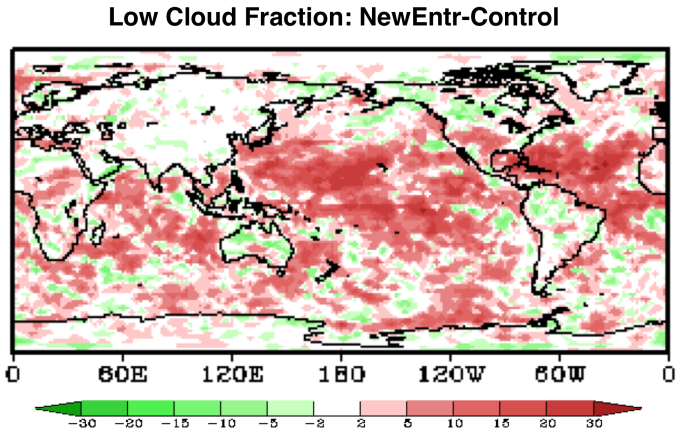

Fig. 11. The difference in low cloud fraction between *NewEntr* and *Control* DA experiments.

GMDD
7, 2249–2291, 2014

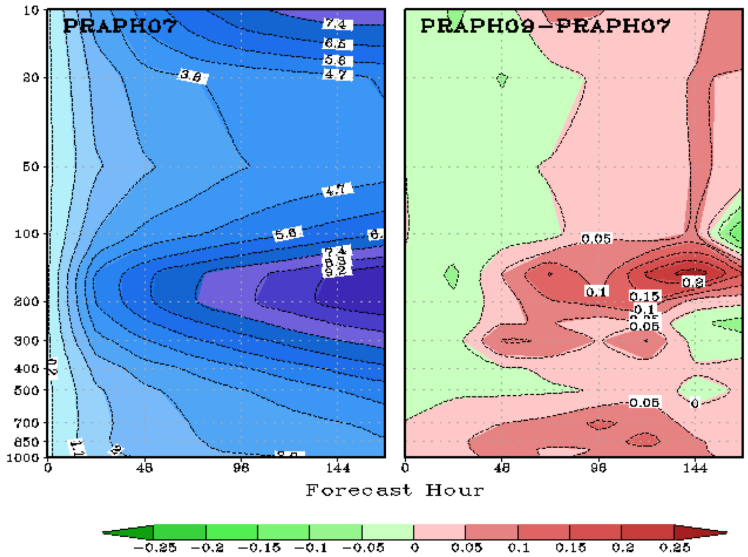

Fig. 12. DA experiments: RMSE in tropical winds in the *Control* DA experiment (left panel), and the change in RMSE in tropical winds between *NewEntr* and *Control*. Colour bar corresponds to the right panel only.

GMDD
7, 2249–2291, 2014